Quantum state transfer in double-quantum-well devices

Jürgen Jakumeit,[a)] Marcel Tutt, and Dimitris Pavlidis
Center for Space Terahertz Technology, Solid State Electronics Laboratory, Deparment of Electrical Engineering and Computer Science, The University of Michigan, Ann Arbor, Michigan 48109-2122

(Received 2 June 1994; accepted for publication 15 August 1994)

A Monte Carlo simulation of double-quantum-well (DQW) devices is presented in view of analyzing the quantum state transfer (QST) effect. Different structures, based on the AlGaAs/GaAs system, were simulated at 77 and 300 K and optimized in terms of electron transfer and device speed. The analysis revealed the dominant role of the impurity scattering for the QST. Different approaches were used for the optimization of QST devices and basic physical limitations were found in the electron transfer between the QWs. The maximum transfer of electrons from a high to a low mobility well was at best 20%. Negative differential resistance is hampered by the almost linear rather than threshold dependent relation of electron transfer on electric field. By optimizing the doping profile the operation frequency limit could be extended to 260 GHz. © *1994 American Institute of Physics.*

I. INTRODUCTION

The quantum state transfer (QST) is a modified form of the RST (real space transfer), first proposed by Hess.[1] Both effects are based on an electric field induced (real space) transfer of electrons from a high-mobility region to a low-mobility region. The transfer of electrons into the low-mobility region increases the resistance and may lead to a negative differential resistance (NDR). The difference between QST and RST mechanisms can be understood by considering the electrons being initially confined in a high mobility quantum well (QW) separated from a low mobility QW through some barrier. In the presence of an electric field the carriers are heated to higher energies and may transfer to the low mobility QW. This transfer may take place in different ways. In the RST the electrons are heated to energies higher than the barrier, and they transfer as classical particles. However, in the case of QST the electron transfer is accomplished by quantum mechanical tunneling through the barrier. Thus electrons need not be heated up to the barrier, instead they can transfer at lower energies than necessary for the RST. Consequently the time the electron system must be heated by an electric field pulse is shorter and the transfer by quantum mechanical tunneling should speed up the characteristics of devices based on this prinicple. In the following we will refer to RST as "electron transfer" for describing the mechanism of electron heating and transfer over a barrier as classical particles.

The possibility of obtaining a NDR by the concept of RST has been investigated by various groups and a number of devices have been proposed based on this principle, such as the charge-injection transistor (CHINT),[2] the negative resistance field-effect transistor (NERFET),[3] and the quantum well emission transistor (QWET).[4] The QST principle has also been explored. Kirchoefer *et al.*[5,6] and Sawaki *et al.*[7–10] provided experimental evidence of NDR in "QST-type" devices. These results do not, however, preclude the possibility of the NDR being due to effects other than the QST, such as the Gunn effect or RST. A special form of the QST, the tunneling real-space transfer (TRST), which uses resonant tunneling of electrons through the barrier, has finally been proposed by Bigelow and Leburton,[11] who presented simulation results for the TRST effect in modulation doped heterostructures.

Although NDR effects can be confirmed by experimental investigations, the study of their origin can greatly benefit from a theoretical analysis. This should allow a physical understanding of the effects taking place in the device and may also be useful in optimizing a structure for a particular operation such as an enhanced NDR. This article presents a simulation of the hot-electron transport in QST devices in view of understanding NDR effects in them. Various double-quantum-well (DQW) structures, optimized in terms of electron transfer and device speed, have been simulated in order to determine criteria for the presence of QST effects.

The simulations described in the article are based on a self-consistent calculation of the conduction band profile, the energy levels, and the wavefunctions. Scattering between the first three subbands in the Γ-valley is considered including acoustic phonon, polar optical phonon, and screened impurity scattering. The results demonstrate the importance of the impurity scattering and the positioning of the subband energy levels for QST operation. Section II gives the theoretical approach used in this work. Examples of intra- and inter-well scattering rates are described in Sec. III. Finally, Sec. IV presents the simulation results for different designs at 77 and 300 K.

II. DOUBLE-QUANTUM-WELL DEVICE STRUCTURE

A typical cross section of the DQW structures (S1) investigated in this work is shown in Fig. 1 together with the contacts necessary for applying an electric field across the GaAs channels. The DQW structure consists of two GaAs layers separated by an $Al_{0.3}Ga_{0.7}As$ barrier. The top GaAs layer is undoped and forms a high mobility channel similarly to a HEMT structure. The design of the corresponding top quantum well (QW) is such that the ground state and the

---

[a)]Permanent address: II. Phys. Inst., University of Cologne, Zülpicherstrasse 77, 50937 Köln 41, Germany.

 0021-8979/94/76(11)/7428/9/$6.00 © 1994 American Institute of Physics

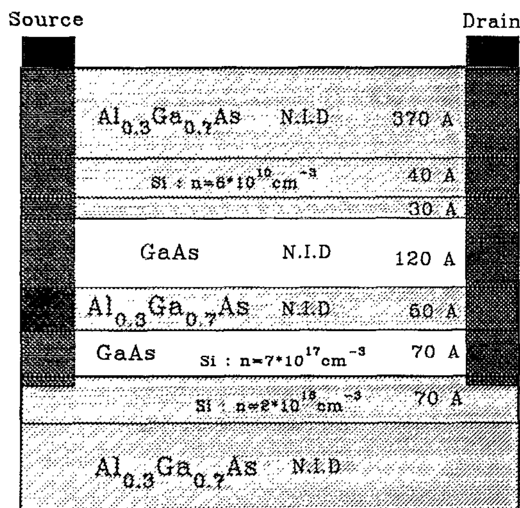

FIG. 1. Cross section of typical DQW structures (S1) studied for QST effects.

second excited state are confined inside this well. Figure 2 confirms this by showing the conduction band profile of the DQW together with the envelope wavefunctions of the first three states. When the electric field applied along the GaAs channels increases, the number of electrons scattered from the ground state into the second subband becomes larger. As shown in Fig. 2, the second subband is confined inside the bottom QW. By designing this QW with a doped GaAs layer it is possible to create a low mobility channel. Based on the above it is evident that by increasing the electric field one may achieve a reduction of the number of electrons in the high mobility region and an increase of them in the bottom QW leading to an overall lower mobility in the device.

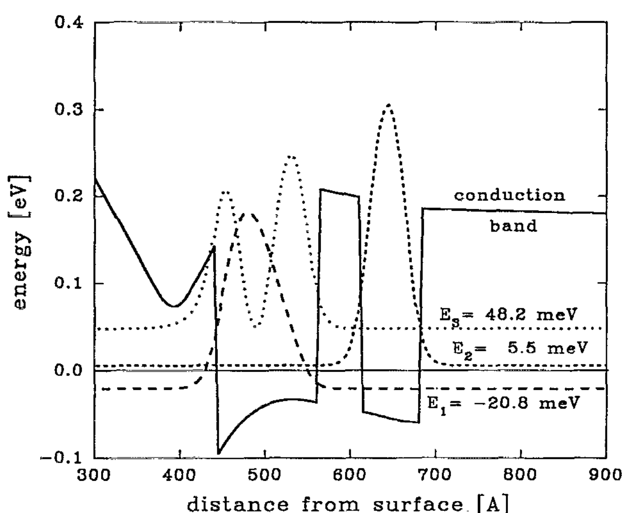

FIG. 2. Conduction band profile and wavefunction of structure S1 calculated at 77 K. The wavefunctions are shifted by the subband energies. The Fermi energy is set to zero.

III. SIMULATION APPROACH FOR TRANSPORT IN DOUBLE QUANTUM WELLS

The procedure followed for simulating the transport properties of the double quantum well structures described in Sec. I consists of three steps. The material parameters used in the simulation are those reported by Adachi.[12]

(i) **Self-consistent solution of Poisson and Schrödinger equations** using a numerical one-dimensional finite-difference method. Ten subbands are considered for the calculation and a constant quasi-Fermi level is assumed across the structure. From the calculations one obtains the conduction band profile, the electron subband energies E_n, the electron wavefunctions $\Psi_n(z)$, and the two-dimensional carrier density in the two QWs. Figure 2 presents the results of the calculation at 77 K for the structure displayed in Fig. 1. The wavefunctions of the first three subbands (shifted by the corresponding subband energy) are shown together with the conduction band diagram of the structure. As discussed earlier, the first and third subbands are well confined in the high-mobility (top) well, while the second subband lies in the doped (bottom) well.

(ii) The **scattering rates** are calculated considering the following scattering mechanisms: acoustic phonon, polar optical phonon, and screened ionized impurity scattering. Since the analysis has been focused on electrons in the Γ-valley, nonpolar optical phonon scattering rates are set to zero. Electron-electron interaction, which leads to an averaging of the electron energies and pushes the energy distribution towards a Maxwellian distribution, should not have a significant effect and has therefore been neglected. As already mentioned only moderate electric fields ($F<2$ kV/cm) are neccessary in QST devices, because electrons must not be heated over the barrier but only to energies, where they can be scattered into the low mobility bottom QW. Such moderate fields should not change the energy distribution of electrons far from a Maxwellian shape even when electron-electron interacton is neglected in a Monte Carlo simulation. The results of our simulation confirm this assumption. The simulation does not include electron-electron interaction but the energy distributions of electrons calculated at 77 and 300 K are, nevertheless, close to a Maxwell distribution. Thus the simplification of neglecting electron-electron interaction does not cause a significant error.

Phonon-electron interaction is calculated following the work of Ridley and Riddoch,[13,14] and phonons are considered "bulk-like." The following formulas have been derived and used for the calculation of scattering from the mth subband to the nth subband:

acoustic phonon scattering:

$$W_{ac}=\frac{\Xi_a^2 k_B T m^*}{4\pi\hbar^3 c_L}\int |G_{n,m}(q_z)|^2 dq_z$$

$$\times G_{n,m}(q_z)=\int_{-\infty}^{\infty}\Psi_n(z)e^{iq_z z}\Psi_m(z)dz, \quad (1)$$

polar optical phonon scattering:

$$W_{po}=\frac{e^2\omega_0}{8\pi^2\epsilon_p}\left(n(\omega_0)+\frac{1}{2}\mp\frac{1}{2}\right)\int_{-\infty}^{\infty}\int_{q_{\min}}^{q_{\max}}\int_0^{\pi}\frac{q}{q^2+q_z^2}$$

$$\cdot|G_{n,m}(q_z)|^2\delta_E\delta_q\theta dq dq_z$$

$$=\frac{e^2\omega_0 m^*}{4\pi\hbar\epsilon_p}\left(n(\omega_0)+\frac{1}{2}\mp\frac{1}{2}\right)$$

$$\times\int\frac{|G_{n,m}(q_z)|^2}{\sqrt{c}}dq_z,$$

$$c=4\hbar^2k^2q_z^2+\hbar^2q_z^4\pm4\hbar m^*\omega^*q_z^2+4m^{*2}\omega^{*2},\hbar\omega^*, \quad (2)$$

$$\hbar\omega^*=\hbar\omega_0\pm(E_m-E_n),$$

where Ξ_a is the acoustic deformation potential, c_L the elastic constant, T the absolute temperature, $\hbar\omega_0$ the longitudinal optical phonon energy, $n(\omega_0)=1/[\exp(\hbar\omega_0/k_BT)-1]$ the number of phonons in the mode, $1/\epsilon_p=1/\epsilon_\infty-1/\epsilon_0$ the effective permittivity (ϵ_∞, ϵ_0 = high-frequency, static permittivity), q_z the phonon wave vector in z direction, q the phonon wave vector in the x,y plane, and k the electron wave vector in the x,y plane.

Ionized impurity scattering is calculated using a screened Coulomb potential[15] and the scattering rates derived in this case are give by:

ionized impurity scattering :

$$W_{\text{imp}}=\frac{e^4m^*}{4\hbar^3\epsilon_0^2}\int_{q_{\min}}^{q_{\max}}\frac{\int N_{\text{imp}}(z_0)M_{mn}(q,z_0)^2dz_0}{q+q_s[1/(1+bq)]}dq,$$

$$M_{mn}(q,z_0)=\int\Psi_n(z)\Psi_m(z)\exp(-q|z-z_0|)dz,$$

$$b=1\Bigg/\left(2\int\Psi_n(z)^2\Psi_m(z)^2dz\right), \quad (3)$$

where $q_s=2\pi e^2n/\epsilon_0k_BT$ is the screening constant (n = 2D carrier density), and $N_{\text{imp}}(z_0)$ is the doping density at z_0.

(iii) A **Monte Carlo simulation** completes the analysis of the DQW structures. A uniform electric field with same value in both wells is assumed for this purpose. Its direction is considered to be parallel to the two wells (x,y plane). As in the step before, the first three subbands of the Γ-valley are considered. Two types of Monte Carlo simulation are used. One is used for the steady state transport properties and the other is used for the evaluation of the time response (speed characteristic) of the structure.

To study the steady state behavior, the motion of one electron is monitored over a long period of time and the corresponding average drift velocity and electron distribution among the three subbands are then calculated. Usually such a "one-electron" simulation is continued until the total number of scattering events exceeds a given value. In the case of this work the main interest lies in the quantum state transfer, which is related with scattering between the two QWs (interwell scattering). The number of scattering events from one QW to the other is therefore more representative of QST than the total number of intrawell and interwell scattering events and has been used as the criterion for determining the duration of the simulation. The simulations revealed that a good convergence in estimating the average electron distribution among the two wells was achieved when the simulations were continued until the electron has transfered 2000 times from one QW to the other.

An ensemble Monte Carlo simulation was used to gain information on both the energy distribution of electrons and speed of the electron transfer. The motion of 5000 electrons was simulated for this purpose and Fermi-Dirac statistics were used to determine the initial electron distribution by assuming that all electrons occupy the first subband. A time discretization scheme of one picosecond was taken and the average number of electrons was stored every 10^{-14} s together with the average electron velocity and the average electron energy in each subband. The value of the electric field could be changed after each time step so that the device response to a variation of the electric field could be investigated.

IV. SCATTERING IN DOUBLE-QUANTUM-WELL STRUCTURES

This section discusses scattering in DQWs and focuses on intra- and interwell scattering rates of structures with possibly enhanced QST characteristics. Structures of various designs have been simulated at 77 and 300 K following the procedure described in Sec. III. The designs have been selected for enhanced QST operation. The speed characteristics of the structures have also been considered in the design. As shown by the simulation discussed in this article, the device performance is mainly determined by four parameters:

(i) the quantum well and barrier thickness,
(ii) the doping of the bottom well and the nearby regions,
(iii) the energy level position, and
(iv) the carrier densities in the high-mobility and low-mobility region.

Table I summarizes the geometries of the structures studied, together with the corresponding doping densities, energy levels, and carrier densities of the top and bottom QW.

As mentioned earlier, our study focuses on scattering between different QWs, rather than between different subbands since the former are indicative of carrier transfer from one well to the other and possibly NDR effects. Scattering from the bottom to the top well can be calculated in a straightforward manner, since the bottom well contains only one subband E_2 (Fig. 2). These interwell scattering rates are determined by adding up the scattering rates from the second E_2 to first E_1 subbands and the second E_2 to third E_3 subbands. The first E_1 and third E_3 subbands are confined in the top well as shown in Fig. 2. Electrons in the top well with an energy higher than the third level can therefore occupy one

TABLE I. Design parameters, energy-levels, and carrier-density solutions for the double quantum well structures considered in this work.

	QW and barrier thickness (Å)			Doping (cm^{-3})	Energy levels (meV) (E_F=0 meV)			Carrier density (cm^{-3}) (F=0 kV/cm)	
	Top	Barrier	Bottom	Bottom well	E_1	E_2	E_3	n_{top}	n_{bottom}
77 K									
S1	120	50	70	7.0×10^{17}	−20.8	5.5	48.2	5.8×10^{11}	1.4×10^{11}
S2	100	50	70	1.5×10^{18}	−20.1	3.2	9.1	6.0×10^{11}	1.0×10^{11}
S3	120	40	65	3.0×10^{18}	−25.6	3.8	41.9	7.8×10^{11}	7.8×10^{10}
S4	120	40	55	6.0×10^{18}	−22.8	5.4	44.3	7.1×10^{11}	8.3×10^{10}
S5	140	60	130	1.0×10^{18}	0.1	14.8	57.7	1.1×10^{11}	3.0×10^{10}
300 K									
S1	120	50	70	7.0×10^{17}	−5.3	65.8	68.6	6.1×10^{11}	5.2×10^{10}
S6	140	50	100	2.5×10^{18}	−3.9	25.3	55.1	5.6×10^{11}	2.3×10^{11}
S7	140	60	90	7.0×10^{17}	−3.5	52.6	56.5	6.2×10^{11}	1.0×10^{11}
S8	140	60	140	7.0×10^{17}	−3.6	35.5	56.7	6.8×10^{11}	1.8×10^{11}

of these two states. The scattering rates for electrons in the top well were considered as an average of the scattering rates for the cases where the first and third subbands act as initial state. This average was calculated assuming that electrons at energies higher than the third level are equally distributed among the first and the third subband as confirmed by Monte Carlo simulations:

$$W_{top\to bottom}(E)=\begin{cases} W_{E_1\to E_2}(E) & E<E_3 \\ [W_{E_1\to E_2}(E)+W_{E_3\to E_2}(E)]/2 & E\geqslant E_3 \end{cases}. \quad (4)$$

Before proceeding to a more detailed study of scattering between the QWs we first analyzed the scattering in the individual QWs. Figure 3 gives the impurity, polar optical phonon, and acoustic phonon scattering rates for scattering inside the top (a) and bottom (b) well for design S1 at 77 K (see Figs. 1 and 2 for structure details). As in all the following figures the electron energy is given with respect to the ground state energy E_1. The impurity scattering, W^b_{imp}, inside the bottom well is more than a factor of ten larger than the impurity scattering in the top well. W^b_{imp} values range from 2×10^{12} to 10×10^{12} s^{-1} and are of the same order of magnitude as the polar optical phonon emission scattering. In fact, impurity scattering dominates the scattering at low energies ($E<E_2+36$ meV) where polar optical emission scattering is not possible. The "HEMT-like" properties of the undoped top well result in a very small total scattering rate for low energies ($E<36$ meV). This is smaller by a factor of 50 than the total scattering rate in the bottom well which unlike the top well consists of a doped GaAs channel. As shown by Fig. 3, electrons with an energy high enough to emit an optical phonon ($E>E_i+36$ meV) are likely to be scattered by phonon emission rather than impurity scattering which is the dominat mechanism at low energies.

The scattering rates into and out of the bottom well are considered next in view of studying the possibility of elec-

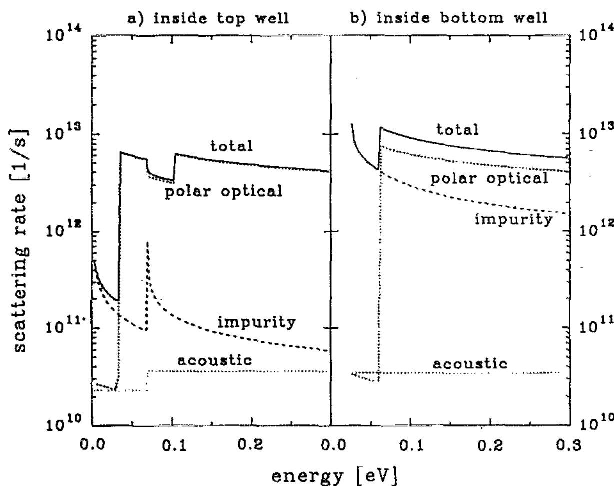

FIG. 3. Impurity, polar optical, and acoustic scattering rates for scattering inside the top (a) and bottom (b) well for structure S1 at 77 K. The ground state energy is set to zero.

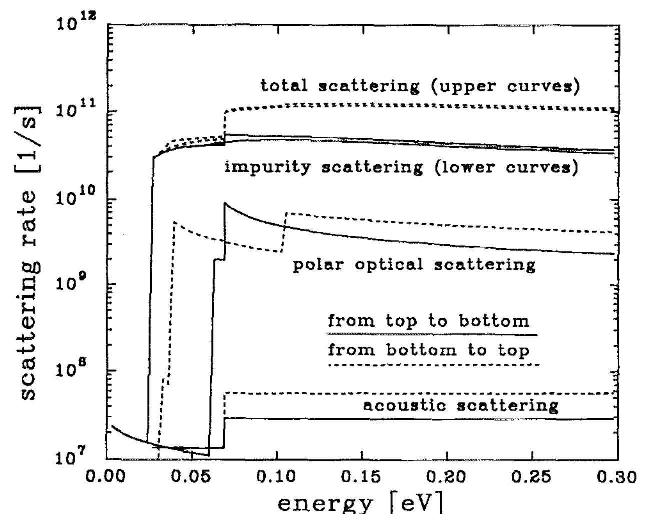

FIG. 4. Interwell scattering rates for structure S1, calculated at 77 K.

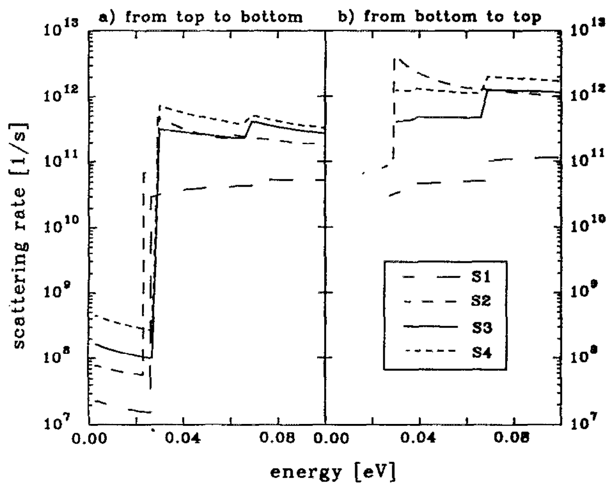

FIG. 5. Comparison of interwell scattering rates for structures S1, S2, S3, and S4. (a) Shows the scattering from top to bottom well and (b) from bottom to top well.

tron transfer. Figure 4 displays such results for design S1. The interwell scattering rates described in this figure are nearly two orders of magnitude smaller than the intrawell ones. Impurity scattering rates, W_{imp}, range from 3×10^{10} to 10×10^{10} s^{-1} and are about one order of magnitude larger than the values related to other mechanisms. In other words, W_{imp} is the dominant mechanism and the total scattering rate is almost equivalent to W_{imp}. The rates for impurity scattering into and out of the bottom well are nearly the same for energies below the third energy level ($E<E_3=69$ meV). However, for higher energies scattering out of the bottom well is two times larger than scattering into the bottom well. This is a result of the fact, that electrons inside the bottom well can scatter into two subbands (1 and 3) while electrons inside the top well have only one subband (2) as their final state.

Figure 5 shows a comparison of the total scattering rates for structures of various designs (including structures S1 for comparison) operated at 77 K. Figure 5(a) shows the scattering rates from the top to the bottom well and Fig. 5(b) shows the scattering rates in the opposite direction. Impurity scattering dominates in all these structures. Structure S2 is designed following the work by Sawaki *et al.*[7–10] and may be viewed as operating close to the resonant tunneling regime, since the energy difference between the second and third subband amounts only to 6 meV in this design. This leads to a higher overlap of the wavefunctions and thus to higher interwell scattering rates. Higher interwell scattering rates lead to a quicker electron exchange between the QWs and should therefore be beneficial to the device speed. Indeed, the interwell scattering rates of design S2 are by more than one order of magnitude higher than those for design S1. The small energy separation results, however, in an undesirable effect namely a pronounced scattering out of the bottom well (b) compared to the other structures. The ratio between the scattering rate into and out of the bottom well $R_{\text{top/bottom}}=W_{\text{top}\rightarrow\text{bottom}}/W_{\text{bottom}\rightarrow\text{top}}$ amounts only to 0.2 for design S2 while structure S1 is characterized by $R_{\text{top/bottom}}\approx1.0$. Monte Carlo simulations revealed that the net result of the lower value of $R_{\text{top/bottom}}$ is a reduced electron transfer. Transferring from the low mobility bottom QW to high mobility top QW competes in this case with the originally intended enhanced transfer from the high to the low mobility QW which is necessary for NDR characteristics.

Similar results for structure S2 must be expected for other structures where resonant tunneling between the two QWs is possible. In the case of resonant tunneling the energy difference between the second and third subband is very small. The solution of Schrödinger's equation does not therefore yield two subbands confined distinctly in one of the channels (see Fig. 1). Instead, two subbands are in this case extended into both QWs and the so-called coherent model describes the operation of such a structure. The description of electrons by such extended subbands is not realistic in practice because of the small dephasing time of the electrons, which hinders the formation of extended states. Picosecond luminescence spectroscopy measurements by Nido *et al.*[16,17] support this by indicating, that even when the two subbands are at resonance the tunneling times are related to scattering processes between subbands which are confined to one rather than two QW. However, recent experiments by Leo *et al.*[18] show, that only under special conditions of low temperature (< 10 K) operation and low carrier density dephasing time becomes long and experimental results can then be interpreted by the coherent model. In DQW structures like S2 the dephasing time is shorter than 10^{-13} s while the resonant tunneling times lie in the picosecond range. Thus, at 77 or 300 K, DQWs with the second and third subband at resonance must be described by nonresonant scattering processes between subbands, confined to one QW. The simulation of structure S2 includes phonon and impurity assisted scattering between such confined subbands. The energy spacing between the two subbands in this structure is small and other designs for further reduction of the energy spacing are not expected to modify the results obtained for this structure significantly. Overall, the simulation of structure S2 can therefore be considered as a representative example for a resonant tunneling structure.

An attempt was also made to increase the interwell scattering by providing a higher doped bottom well, as well as, by doping at the same concentration the barrier at the interface to the bottom well over a region of 20 Å. The upper part of this barrier near the top well remained undoped. Typical designs with such features are noted by structure S3 and S4. In those designs $n_{\text{doping}}=3\times10^{18}$ cm^{-3} (S3) and $n_{\text{doping}}=6\times10^{18}$ cm^{-3} (S4) was chosen for the bottom well (see Table I). Figure 5 shows that the enhanced doping of the bottom well and nearby regions increases the scattering rate from the high mobility top to the low mobility bottom of design S3 by more than one order of magnitude ($W_{\text{top}\rightarrow\text{bottom}}\approx2\times10^{11}$ s^{-1}) and those of design S4 even by a factor of 40 ($W_{\text{top}\rightarrow\text{bottom}}\approx8\times10^{11}$ s^{-1}) compared with design S1. An important result is that the higher doping increases both the scattering rate into and out of the bottom well by almost the same factor. Thus the ratio between the scattering rate into and out of the bottom well $R_{\text{top/bottom}}$ is not significantly lowered by the enhanced doping of the bot-

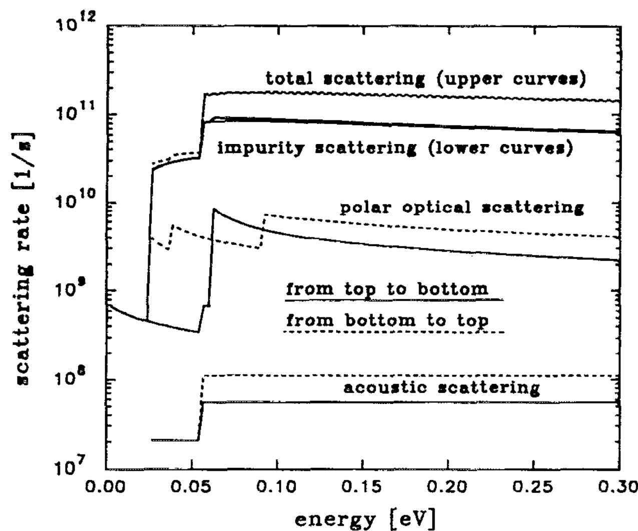

FIG. 6. Interwell scattering rates for structure S6, calculated at 300 K.

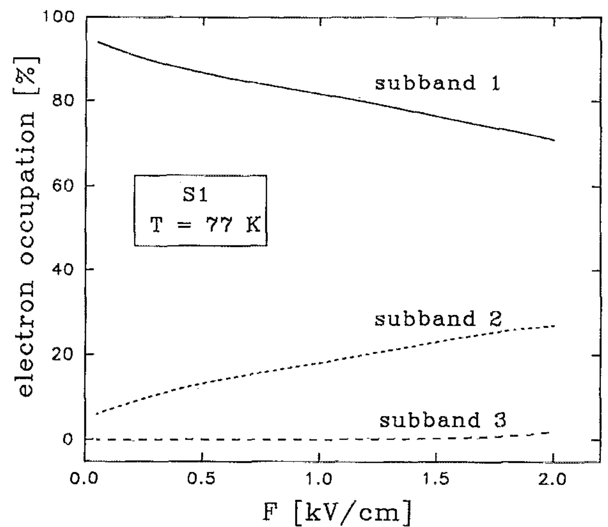

FIG. 7. Electric field dependence of the electron occupation in the first three subbands of structure S1 (T = 77 K).

tom well and the barrier. Design S3 is still characterized by $R_{top/bottom} \approx 0.75$. The high doping in structure S4 reduces $R_{top/bottom}$ already to 0.6 but this value is still much better than the low value of $R_{top/bottom} \approx 0.2$ obtained for structure S2. Enhancing the interwell scattering rates by a higher doping of the bottom well and nearby regions is therefore much more promising than the resonant tunneling idea.

Although up to this point the structures discussed have been evaluated at 77 K similar scattering rate results are obtained when calculated at 300 K. The main difference compared to 77 K operation concerns the polar optical absorption scattering which is larger and of the same order of magnitude as the polar optical emission scattering due to the much higher phonon occupation number $n(\omega_0)$ at 300 K. Comparison of scattering rates of a design operated at 77 and 300 K are of no special importance since the energy levels shift considerably with temperature (see Table I). By way of an example, structure S1, which was originally designed for 77 K operation with a large energy gap between the second and third subbands, results at 300 K in a very small second to third level separation and has consequently features which reassemble those of the resonant tunneling concept. In structure S6, calculated at 300 K, the arrangement of energy levels is comparable to structure S1 at 77 K. The second subband lies here about 26 meV above the ground state. The interwell scattering rates of this structure at 300 K are shown in Fig. 6. A comparison with Fig. 4 (S1 calculated at 77 K) reveals that the scattering rates are of the same order. Again, the impurity scattering dominates the scattering over the entire energy range.

In summary, the investigation of the interwell scattering rates revealed that impurity scattering is the dominant mechanism for the QST. Furthermore, an enhanced doping of the bottom well and nearby regions, as well as, a small energy separation between the second and third subband lead to a significant increase of interwell scattering. The latter, however, yields a much higher scattering out of the bottom well than into the bottom well and consequently conflicts with the QST idea.

V. MONTE CARLO SIMULATION OF TRANSPORT IN DOUBLE QWS

The DQW designs studied in Sec. IV, as well as some others (see Table I for design details) have been investigated from the point of view of their transport properties using the Monte Carlo (MC) technique outlined in Sec. III. As for the previous studies the goal of the analysis has been quantum mechanical tunneling of electrons from a high to a low mobility QW induced by an electric field. The MC simulation considered only Γ-valley states and is only valid up to electric fields of about 2 kV/cm; at higher fields the electrons gain more energy from the electric field than they lose by polar optical emission scattering and the simulation does not converge. Such a high field excitation would result in L-valley transfer which is not accounted for by our model.

The change of electron occupation in each of the three subbands of structure S1 at 77 K is displayed in Fig. 7. By increasing the electric field from 0 to 2 kV/cm the number of electrons in the second subband, i.e. the bottom well, increases from 7% to 27% and the number of electrons in the first subband decreases correspondingly. The occupation of the third subband is always below 1% and this state plays no role in the electron transfer. At 77 K, such a negligible low electron occupation is characteristic for states having an energy higher than the optical phonon energy (36 meV). The polar optical phonon emission scattering rate in the top well is more than one order of magnitude larger than the other scattering rates (see Fig. 3). Electrons with $E>36$ meV are very likely to emit a phonon and scatter back to low energies. Electrons can therefore hardly reach high enough energies to scatter into subbands above 36 meV and even if they do so, they are likely to scatter out of these states. Based on the above, it is evident that DQW structures cannot show a significant electron transfer if the second subband (characteristic of carriers confined in the bottom well) lies above the threshold of the polar emission scattering.

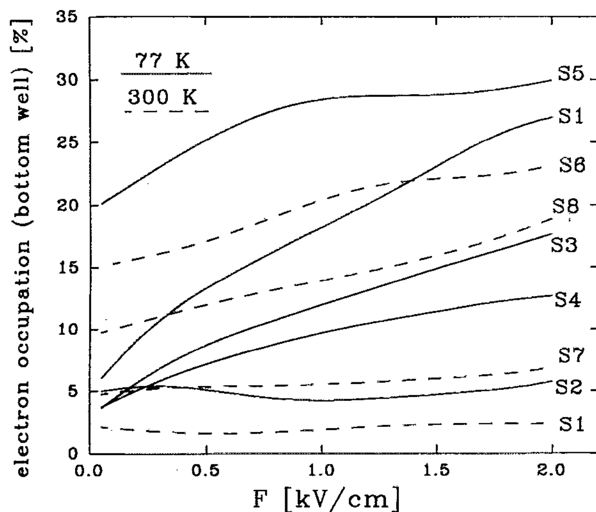

FIG. 8. Electron occupation of the low mobility well as a function of electric field for different structures simulated at 77 K (solid lines) and 300 K (dashed lines).

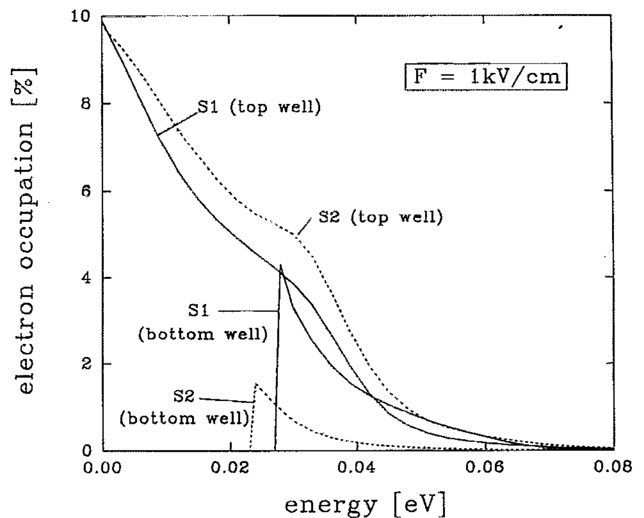

FIG. 9. Comparison between the energy distribution of carriers inside the top and bottom well for structures S1 and S2.

The magnitude of electron transfer can be directly estimated by the change of the electron occupation in the top or bottom well with increasing electric field. Figure 8 displays this change for the electron occupation of the bottom well of various designs. The results are presented for 77 K (solid lines) and 300 K (dashed lines) operation. The largest electron transfer obtained occurred for structure S1 and resulted in a change of electron population by 20%.

Structure S5 has been designed with the second subband lying only 15 meV above the ground state. Figure 8 shows that the second subband (bottom well) has the highest electron occupation of all structures considered. The small energy separation between the first and second subband is responsible for this high occupation which reaches 20% even at zero electric field. At electric fields above 1 kV/cm, the electron occupation of the bottom well saturates at 30%. Thus the overall electron transfer reaches only 10%. The decrease of the second subband energy from 26 meV (S1) to 15 meV (S5) reduces the electron transfer from 20% to 10%.

The simulation results of structure S2 demonstrates that electron transfer is almost zero in designs, which are characterized by a very small energy separation between the second and third level and come close to the resonant tunneling regime. Doping of the bottom well combined with an appropriate energy level alignment leads to strong impurity scattering of electrons out of the bottom well as, for example, shown by the results of Fig. 5. This results in a short dwell time for electrons in the bottom well. Consequently, the average number of electrons in this well becomes also very low. This result is demonstrated in Fig. 9. Here, the energy distribution of electrons at an electric field of 1 kV/cm is plotted for structures S1 and S2. In the case of structure S1 the electrons at high energies are almost equally distributed among the top and bottom well, but in structure S2 the number of electrons occupying the bottom well remains insignificant.

On the other hand increasing the interwell scattering rates by an enhanced doping of the bottom well and nearby regions is possible as structures S3 and S4 demonstrate. Both structures are characterized by high interwell scattering rates (see Fig. 5), but the real space transfer does not vanish as shown by the resuts of Fig. 8. The electron transfer reaches 15% in structure S3 and still 10% of all electrons transfer to the bottom well in structure S4, where the higher doping of the bottom well leads to a larger scattering rate out of it.

Furthermore Fig. 8 demonstrates that similar effects to those found for 77 K operation can also be observed at 300 K. By simulating at 300 K designs, where the energy separation between the second and third subbands is very small, [see, for example, S1 and S7 ($\Delta E < 4$ meV)], one again finds no electron transfer. Structures S8 and S6, where the energy separation between second and third subband is larger than 20 meV, reveal a small electron transfer of about 8%. Since the heating of the electron gas at a lattice temperature of 300 K is less effective than at 77 K, it is not surprising that the electron transfer is smaller at 300 K, i.e., maximum transfer of 8% at 300 K compared to 20% at 77 K.

The possibility of NDR being present in the designs discussed above has been investigated by examining the electric field dependence of the drift velocity. The results are shown for all the designs investigated in Fig. 10. Design S1 operated at 77 K, which has the largest electron transfer of 20%, develops no NDR effects for the ensemble of the two quantum wells. The overall mobility is, however, reduced drastically upon the application of a modest electric field due to the increased occupation of the low mobility bottom well. The smaller electron transfer in structure S3, combined with a higher doping and thus lower mobility of the bottom well, results in a comparable mobility drop but yields no NDR, either. The small mobility drop in structure S2 is due to enhanced polar optical phonon emission scattering of the heated electrons. The much stronger reduction of the mobility in structures S1 and S3 is caused by the QST. Structure S4 reveals a mobility drop which is lower than that of struc-

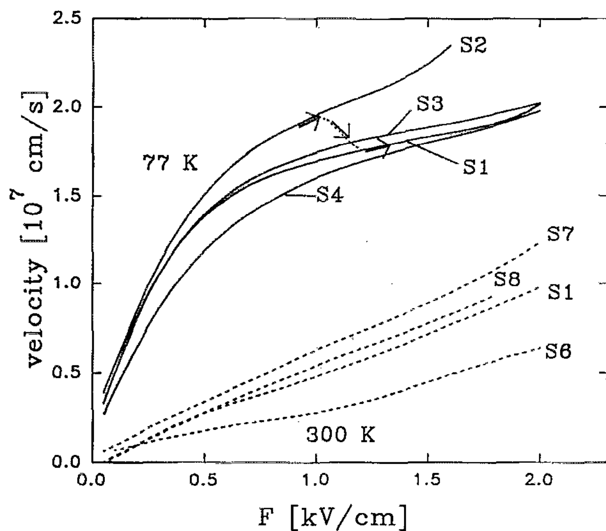

FIG. 10. Electric field dependence of the drift velocity for different structures, simulated at 77 K (solid lines) and 300 K (dashed lines).

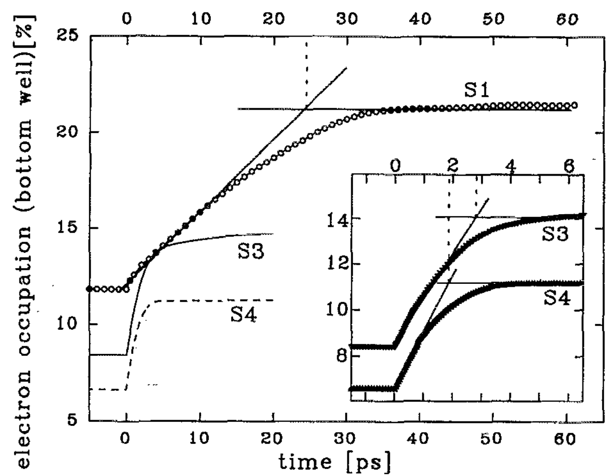

FIG. 11. Change of the electron occupation in the bottom well for structures S1, S3, and S4 at 77 K in response to an electric field change with ideal (zero) risetime. The electric field was change at $t=0$ ps from 0.5 kV/cm to 1.5 kV/cm.

tures S1 and S3 but still significantly larger than in structure S2.

For 300 K, Fig. 10 shows for all structures (dashed lines) a much smaller mobility drop than for 77 K, due to the smaller electron transfer at this temperature, as discussed in Fig. 8. The small electron transfer present in structures S8 and S6 unfortunately does not lead to a significant mobility drop. Structures S1 and S7, which show no electron transfer, are characterized by a small curvature of velocity with electric field. The increase of the polar optical phonon scattering with higher electrical fields appears to be responsible for these characteristics.

The results of Fig. 10 suggest that the presence of NDR requires either much larger electron transfer, or transfer initiated above some distinct electric field strength associated with a threshold value for such effects to occur. To analyze the latter possibility we assume that the electron transfer between the two QWs in structure S1 is initiated and completed between 1.0 kV/cm and 1.2 kV/cm instead of changing linearly with the electric field (see arrows in Fig. 10). For fields below 1.0 kV/cm the velocity/field characteristics of design S1 would then be similar to those of structure S2, which shows no real space transfer. Above 1.2 kV/cm the velocity/field characteristics will reassemble with those of the original simulated characteristics. Figure 10 demonstrates that this would lead to a strong drop within the small electric field range and would yield a NDR as indicated by the hypothetical dashed curve and the arrows. However, the NDR does not appear due to the almost linear dependence of the electron transfer with the electric field in QST structures.

The ensemble Monte Carlo technique was finally used to simulate the response of the DQW structures to ideal (zero rise time) electric fields changes. Figure 11 compares the change of the electron occupation of the bottom well for structures S1, S3, and S4 in response to a zero rise time electric field change from 0.5 kV/cm to 1.5 kV/cm at $t=0$ ps. The electron system of the DQWs of structure S1 needs about 25 ps to completely respond to the electric field change. Structure S3 reaches equilibrium after 2.8 ps electric field pulse duration while the response time τ of structure S4 is only 1.9 ps (see inset of Fig. 11). Simulations with different electric field values in the range 0.5 kV/cm–1.5 kV/cm revealed that τ does not significantly depend on the field strength. In addition, τ remains almost the same for each design if the electric field is not increased from 0.5 kV/cm to 1.5 kV/cm but decreased from 1.5 kV/cm to 0.5 kV/cm.

An estimation of the frequency limit of the structures can be obtained by assuming $f_{\max}\approx 1/(2\cdot\tau)$. The formula yields frequency limits of 20, 180, and 260 GHz for structures S1, S3, and S4, respectively. It appears from the design corresponding to these structures that the device speed can consequently be drastically increased by doping the bottom well and the barrier near the bottom well. Since the energy difference between the first and second subband is almost identical for designs S1, S3, and S4, the increase in the device speed can be directly linked to the higher interwell scattering rates of structures S3 and S4. The ten times higher interwell scattering rates of structure S3 compared with structure S1 lead to an almost ten times higher frequency limit. Such a proportionality was not found for structure S4 which has more than 40 times higher interwell scattering rates but only a 15 times higher frequency limit. An investigation of the electron heating in the top well reveals that the electron gas inside the top well needs about 1 ps to respond to the electric field change. Thus the device speed of structure S4 is not only limited by the electron scattering between both wells but also by the heating and relaxation time of the electron gas in the top well. Using the energy heating time of 1 ps as a time dictating the upper limit of operation frequency, a maximum frequency of 500 GHz could be estimated for QST devices. Finally, structure S5 demonstrates that it is not possible to overcome this limitation by a further reduction of the energy separation between the first and second subband, since this would lead to a reduced real space transfer as demonstrated by the results of Fig. 8.

VI. CONCLUSIONS

A complete simulation of QST devices, including acoustic phonon, polar optical phonon, and screened impurity scattering has been presented. Impurity scattering is demonstrated to play an important role in the electron transfer. The possibility of QST operation was investigated by simulating structures optimized in terms of magnitude and speed of the electron transfer. The simulations have revealed basic physical limitations in QST devices.

The occupation of the low mobility state did not exceed 30% and the maximum transfer of electrons from a high mobility to a low mobility well was at best 20%. Even for an optimized design, such as S1, a NDR due to the QST effect was not observed. The fact that the electron transfer from the high to the low mobility well increases almost linearly with increasing electric field reduces the possibility of a NDR.

In the case of Gunn effect and RST operation an electric field threshold exists, above which the electrons are no longer at equilibrium in the QW. Above this critical field carriers are transferred to the L-valley or cross over a barrier into a collector layer; this threshold yields an abrupt onset of the electron transfer. In QST operation the energy distribution of electrons is smoothly changed with the electric field and leads to the observed almost linear electric field dependence of the electron transfer. Designs such as S1 or S3, which show enhanced electron transfer, could have NDR characteristics if the onset of this transfer was abrupt.

The simulations also revealed that in structures, where, following the resonant tunneling idea, the energy separation between the second and third subband is small, the enhanced impurity scattering out of the low mobility region prevents a significant electron transfer. Thus it is not possible to speed up the device by bringing the second and third subband close together.

On the other hand, the device operation frequency can be increased up to 200 GHz by an optimized doping of the bottom well and parts of the barrier. This approach resulted in frequency limits of 180 and 260 GHz for structures S3 and S4, respectively. The frequencies are already close to the limit of about 500 GHz given by the electron heating and relaxation time inside the top QW.

The advantage of the QST effect compared with the RST or Gunn effect is, that electrons can transfer at lower energies resulting, therefore, in reduced heating and relaxation times. The results of designs S3 and S4 demonstrate that it is possible to make use of this advantage, if the transfer times (interwell scattering times) are reduced by optimum doping. The presented simulations show that the QST effect is a promising base for high frequency devices, if NDR effects can be induced by QST operation. This may be possible by using more complex multi-quantum-well designs instead of the simple DQW designs, investigated here.

ACKNOWLEDGMENTS

The very useful and constructive suggestions of Professor K. Tomizawa regarding this work are greatly acknowledged. Thanks are also due to Professor Nimtz for his continuous encouragement. This work was supported by NASA Contract No. NAGW 1334 and URI-ARO Contract No. DAAL03-92-G0109.

[1] K. Hess, H. Morkoç, H. Shichijo, and B. G. Streetman, Appl. Phys. Lett. **35**, 469 (1979).
[2] A. Kastalsky and S. Luryi, IEEE Electron. Dev. Lett. **EDL-4**, 334 (1989).
[3] S. Luryi, A. Kastalsky, A. Gossard, and R. Hendel, IEEE Trans. Electron Devices **ED-31**, 832 (1984).
[4] K. Hong and D. Pavlidis, J. Appl. Phys. **69**, 2662 (1991).
[5] S. W. Kirchoefer, R. Mango, and J. Comas, Appl. Phys. Lett. **44**, 1054 (1984).
[6] J. M. Pond, S. W. Kirchoefer, and E. J. Cukauskas, Appl. Phys. Lett. **47**, 1175 (1985).
[7] N. Sawaki and I. Akasaki, Physica **134B**, 494 (1985).
[8] N. Sawaki, M. Suzuki, Y. Takagaki, H. Goto, I. Akasaki, H. Kano, Y. Tanaka, and M. Hashimoto, Superlatt. Microstruct. **2**, 281 (1986).
[9] H. Kano, Y. Tanaka, N. Sawaki, M. Hashimoto, and I. Igarashi, J. Cryst. Growth **81**, 144 (1987)
[10] N. Sawaki, M. Suzuki, E. Okuno, H. Goto, I. Akasaki, H. Kano, Y. Tanaka, and M. Hashimoto, Solid-State Electron. **31**, 351 (1988).
[11] J. M. Bigelow and J. P. Leburton, Appl. Phys. Lett. **57**, 795 (1990).
[12] S. Adachi, J. Appl. Phys. **58**, R1 (1985).
[13] B. K. Ridley, J. Phys. C **15**, 5899 (1982).
[14] F. A. Riddoch and B. K. Ridley, J. Phys. C **16**, 6971 (1983).
[15] P. J. Price, J. Vac. Sci. Technol. **19**, 599 (1981).
[16] M. Nido, M. G. W. Alexander, W. W. Rühle, and K. Köhler, SPIE **1268**, 177 (1990).
[17] M. G. W. Alexander, M. Nido, W. W. Rühle, and K. Köhler, Phys. Rev. B **41**, 12295 (1990).
[18] K. Leo, J. Shah, E. O. Göbel, J. P. Gordon, and S. Schmitt-Rink, Semicond. Sci. Technol. **7**, B394 (1992).